Hindawi
Geofluids
Volume 2017, Article ID 9568349, 11 pages
https://doi.org/10.1155/2017/9568349

WILEY | Hindawi

Research Article

Applying Environmental Isotope Theory to Groundwater Recharge in the Jiaozuo Mining Area, China

Pinghua Huang and Xinyi Wang

School of Resources and Environment Engineering, Henan Polytechnic University, Jiaozuo 454000, China

Correspondence should be addressed to Pinghua Huang; hph2001@hpu.edu.cn

Received 29 January 2017; Revised 28 March 2017; Accepted 23 April 2017; Published 22 May 2017

Academic Editor: Nerantzis Kazakis

This study establishes the surface water evaporation line in theory and numerically simulates the δD and δ^{18}O value distribution interval of the recharge source of deep groundwater in the Jiaozuo mining area. The recharge elevation is calculated based on hydrogen and oxygen isotope tracer theory. Theoretical calculation and experimental data indicate that the surface water evaporation line in the study area in theory is almost the same as the measured surface data-fitting line. A significant linear relationship is identified between δ^{18}O and the elevation of spring outcrop. The topography increases per 100 m, and the δ^{18}O value reduces by 0.23‰ on average. The δ^{18}O value is converted into formula to calculate the groundwater recharge elevation, which is approximately from 400 to 800 m. The measured tritium values of karst groundwater are greater than 3 TU. The second factor score is a fraction distribution in shallow groundwater and negative fraction distribution in spring and deep groundwater, which indicates that the Northern Taihang Mountain is the main recharge area, where carbonate-exposed areas exist. The research conclusion holds a certain value for the flood evaluation of local coal mines.

1. Introduction

Jiaozuo belongs to the warm semihumid, semiarid continental monsoon climate zone. The average annual precipitation is less than 600 mm, yet the evaporation is higher than 2000 mm [1]. The evaporation is thrice that of the precipitation. Nevertheless, karst water is very rich in the Jiaozuo Coal Mine District. Jiaozuo is one of the most famous mining districts with karst water inrush; heavy, large water inrush accidents are frequent. Some disputes contest the recharge sources of karst water in the mining area. For example, Pei and Tong [1] believed that karst water comes mainly from local rainfall infiltration recharge. On the contrary, the current study simulates the recharge source of karst water by hydrogen and oxygen isotope-tracing theory. The result shows that other major recharge sources of groundwater exist in the mining area. This conclusion holds a certain value for the hazard assessment of local coal mines.

The isotope tracer technique began in the 1950s; it is applied to the field of hydrology, but it is limited to the study of artificial isotope tracing. In the late 1960s, isotope was widely used in hydrology research [2–5]. The wide application of isotope becomes possible with the improving hydrogen and oxygen isotope test technology and the reducing testing cost in recent years. Isotope plays its unique advantages in the aspects of research on groundwater formation mechanism and supply mechanism. In foreign countries, hydrogen and oxygen isotopes are used to study groundwater [2–10].

In China, hydrogen and oxygen isotopes also show unique advantages in mine groundwater tracer. Gui et al. [11] studied the composition and drift characteristics of hydrogen and oxygen stable isotopes in groundwater and accurately identified the recharge source of groundwater in the Wanbei mining area with the hydrogen and oxygen stable isotope tracer technology. Chen et al. [12] studied the isotope composition of the surface water and groundwater in Ren Lou and the Linhuan mining area and analyzed the possible groundwater recharge sources. The result indicated that groundwater flowed relatively fast, and the drift phenomenon was insignificant. Dou et al. [13] surveyed the mine water

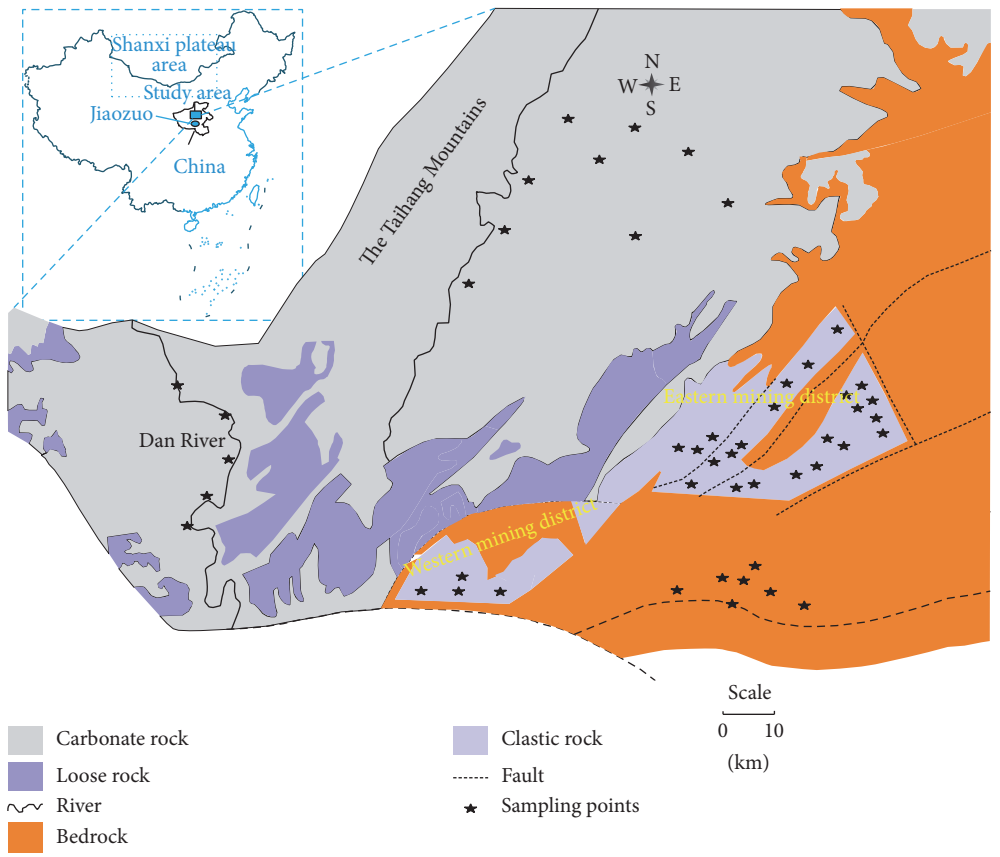

Figure 1: Hydrogeological map of the Jiaozuo coal-mining district in China.

supply source using the hydrogeochemical technology by analyzing the isotope and hydrochemical characteristics of surface water and groundwater from different aquifers. The results showed that the groundwater isotopic and hydrochemical characteristics in the Cretaceous aquifer were similar to leaking groundwater from the 73,003 work face. The groundwater of the Cretaceous conglomerate aquifer is the major source of water inrush, which accounted for 67% of the proportion, and the Quaternary groundwater accounted for 33%. Wang and Li [14] studied the hydrogen and oxygen isotope composition and distribution characteristics of groundwater in the Pingdingshan mining area to identify the groundwater flow system, which was divided into two flow subsystems, namely, local flow system and excessive water system. A method for determining the groundwater recharge source was provided.

2. Hydrogeological Setting

The Jiaozuo mining area is located in the northern part of the Henan Province and the adjacent Shanxi Plateau (Figure 1). The Taihang Mountain uplift belt in the southeast edge of the wing front arc, the East New Cathaysian tectonic system, and the Qinling Mountains weft composite parts comprise the structural system of the Jin East Nanshan-type tectonic system. Faults and folds are not well developed. The monocline of the general tendency to southeast is determined. The fault structure mainly consists of high-angle normal faults, including the North East, Near East, and North West, especially in the development of the North East. The developing faults not only control the distribution and occurrence features of coal seam, but also form a natural boundary area of minefield. The limestone aquifer is the deposition base of coal measure strata, which is also the main source of water inrush in the coal seams with very rich karst water storage.

The main aquifers, from top to bottom, can be divided into four categories according to the lithology, thickness, water features, and burial conditions of the stratum. The first category is the Quaternary aquifer that is made up of the Quaternary sandstone, clay, calcareous nodules, and the conglomerate bottom, which is the main aquifer for the segment. The second category is the coal-bearing sandstone aquifer that consists of sandstone, siltstone, and shale layers with permeability (K) of 0.1 to 0.3 m/d. The third category is the Carboniferous limestone aquifer composed of Taiyuan limestone. The main fractured karst aquifer in this district features a stable distribution of limestone karst subaquifers. Pumping tests in the drilling borehole reveal that the aquifer permeability is approximately 1 to 3 m/d. The fourth category is the Ordovician limestone aquifer that is the sedimentary basement of the coal measure strata; its

lower layer is composed of thick gray limestone with a few brecciated limestones and yellow-green marls, and its upper layer consists of gray or dark gray thick-bedded limestone and dolomitic limestone with a few thin-bedded limestones. The aquifer permeability is approximately 1 to 30 m/d. The karst water level of the Ordovician limestone aquifer implies that the karst water level gradually increases from the coal-mining district northward to the Taihang Mountains [15].

3. Materials and Methods

3.1. Sampling and Analytical Methods. Forty-nine groups of water samples were collected from the coal-mining district in August 2008 and October 2008, including 9 groups of river samples, 12 groups of shallow groundwater samples taken by pumping from the wells of the Quaternary aquifer, 7 groups of spring water samples from the northern mountainous area, and 21 groups of deep groundwater samples taken by pumping from the boreholes of the coal-bearing sandstone aquifer, Carboniferous limestone aquifer, and Ordovician limestone aquifer. The pH values of water samples were determined with a WM-22EP on site. Water samples were determined at State Key Laboratory of Hydrology-Water Resources and Hydraulic Engineering, Hohai University. Hydrogen isotopes were determined by using the zinc reaction method, and oxygen isotope was determined with the oxygen-carbon balance method. The measuring results of the MAT253 isotope mass spectrometer instrument involved the Vienna Standard Mean Ocean Water with thousand poor representation. The determined accuracy for hydrogen and oxygen was 0.2‰ and ±0.1%, respectively. Radioactive tritium was determined by using Tri-Carb 3170TR/SL with accuracy of 0.1‰ (Table 1). The chemical composition of water samples was determined in the State Key Laboratory of Hydrology using a Shimadzu CTO-10 Avp ion chromatograph and inductively coupled plasma mass spectrometry with a relative error of 1%, and HCO_3^- was determined using the method of dilute sulfuric acid–methyl orange titration (Table 2).

3.2. Factor Analysis. Factor analysis method is a multivariate statistical analysis technique, which is used to reduce the data and the study dependencies among variables and to explore the basic structure of the observational data that are expressed by several factors that can reflect the main message that most of the observed variables contain and explain the interdependent relationship among these observed variables. The loadings describe the proportion of each individual sample that is necessary to project the variables onto the factor axis as opposed to describing the proportion of each variable used to project each sample onto the factor axis, as in R-mode analysis [16, 17]. The method plays a key role in the assessment of surface water-groundwater interaction [18–21]. In this study, the factor analysis method is applied by the principal component analysis technique. The common factors can be determined when the eigenvalue is usually greater than 1 and the cumulative contribution rate is as large as possible. The actual meaning of common factors is determined according to the loading of the observations that represent the correlation coefficient between analysis variables and the common factors.

4. Results

4.1. Theory Evaporation Line. In studying groundwater recharge, the surface water evaporation line is an important reference, which can be obtained by fitting the measured data; however, the cost is high given the measured large amounts of data [22, 23]. Therefore, this study combines the theoretical and measured values to calculate the surface water evaporation line. During water evaporation, the hydrogen and oxygen stable isotopic fractionation mainly includes two parts, namely, dynamic fractionation and balance fractionation. Humidity and temperature are the main factors affecting isotopic fractionation. The residual water isotope ratio and evaporated water vapor isotope ratios follow the Rayleigh fractionation model. The following types are established:

$$\frac{\delta^{18}\mathrm{O} + 1000}{\delta^{18}\mathrm{O}_0 + 1000} = f^{\alpha^* - 1} \quad \text{or} \quad \frac{\delta\mathrm{D} + 1000}{\delta\mathrm{D}_0 + 1000} = f^{\alpha^* - 1}, \tag{1}$$

$$S = \frac{24.844\left(10^6/(T+273)^2\right) - 76.248\left(10^3/(T+273)\right) + 52.612 + 12.5(1-h)}{1.137\left(10^6/(T+273)^2\right) - 0.4156\left(10^3/(T+273)\right) - 2.0667 + 14.2(1-h)}, \tag{2}$$

$$\delta\mathrm{D} = \left(\delta\mathrm{D}_0 + 1000\right) \cdot \left(\frac{\delta^{18}\mathrm{O} + 1000}{\delta^{18}\mathrm{O}_0 + 1000}\right)^{(24.844(10^6/(T+273)^2) - 76.248(10^3/(T+273)) + 52.612 + 12.5(1-h))/(1.137(10^6/(T+273)^2) - 0.4156(10^3/(T+273)) - 2.0667 + 14.2(1-h))} - 1000, \tag{3}$$

Table 1: Isotopic composition of all water samples in the study area.

Number	Type	$\delta^{18}O$ (‰)	δD (‰)	^{3}H (T.U.)	D-excess	Factor 1 score	Factor 2 score	Factor 3 score
1	Spring	−8.85	−63.61	8.23	7.19	−0.59	−0.09	−0.58
2	Spring	−8.73	−58.88	7.29	10.96	−0.61	0.13	−0.65
3	Spring	−9.21	−67.61	8.65	6.07	−0.80	−0.14	−0.72
4	Spring	−8.77	−66.34	7.35	3.82	−0.60	−0.12	−0.35
5	Spring	−8.81	−61.6	9.35	8.88	−0.79	0.16	−0.53
6	Spring	−8.81	−62.39	8.05	8.09	−0.82	0.08	−0.59
7	Spring	−8.69	−70.43	8.58	−0.91	−0.41	−0.36	1.21
8	Shallow groundwater	−7.67	−60.92	9.44	0.44	1.67	0.17	4.03
9	Shallow groundwater	−7.26	−53.1	8.99	4.98	1.69	0.67	−0.57
10	Shallow groundwater	−8.31	−67.28	10.8	−0.8	0.66	−0.40	3.22
11	Shallow groundwater	−4.07	−28.76	9.59	3.8	−0.38	2.52	−0.16
12	Shallow groundwater	−6.61	−48.4	11.89	4.48	−0.76	1.30	0.15
13	Shallow groundwater	−8.2	−62.8	9.41	2.8	0.17	0.08	0.87
14	Shallow groundwater	−7.88	−59.1	12.38	3.94	−0.98	0.71	−0.47
15	Shallow groundwater	−8.52	−65.88	6.52	2.28	0.23	−0.30	0.11
16	Shallow groundwater	−8.21	−61.48	10.54	4.2	−0.70	−0.35	1.41
17	Shallow groundwater	−8.43	−66.75	7.65	0.69	−0.73	−0.19	0.07
18	Shallow groundwater	−8.9	−67.58	6.18	3.62	0.24	−0.21	1.22
19	Shallow groundwater	−8.89	−66.16	6.69	4.96	−0.19	−0.33	−0.28
20	River	−8.57	−67.94	9.85	0.62	−0.70	−0.01	0.25
21	River	−8.29	−61.97	8.59	4.35	−0.58	0.28	−0.92
22	River	−8.08	−55.7	13.17	8.94	−1.15	0.81	0.05
23	River	−7.99	−56.48	10.91	7.44	−1.02	0.74	−0.51
24	River	−8.78	−57.42	7.05	12.82	−0.47	−0.03	−0.28
25	River	−7.77	−56.7	13.46	5.46	−0.82	0.96	0.66
26	River	−8.63	−66.59	9.35	2.45	−0.34	0.03	0.78
27	River	−8.05	−61.84	12.11	2.56	−0.12	0.90	0.28
28	River	−8.43	−62.54	8.53	4.9	−0.27	0.12	0.66
29	Deep groundwater	−9.17	−65.61	7.68	7.75	−0.63	0.21	−0.51
30	Deep groundwater	−9.37	−62.91	7.2	12.05	−0.26	−0.51	0.15
31	Deep groundwater	−8.76	−66.19	6.07	3.89	−0.08	−0.26	−0.71
32	Deep groundwater	−9.36	−60.89	5.65	13.99	−0.25	−0.48	−0.26
33	Deep groundwater	−8.99	−66.5	7.65	5.42	−0.42	−0.10	−0.73
34	Deep groundwater	−9.45	−67.23	7.43	8.37	0.65	−0.66	−0.66
35	Deep groundwater	−9.23	−66.59	6.38	7.25	0.38	−0.40	−0.93
36	Deep groundwater	−9.04	−69.72	7.51	2.6	−0.65	−0.20	−0.41
37	Deep groundwater	−9.03	−70.15	6.01	2.09	−0.28	−0.64	−0.26
38	Deep groundwater	−9.26	−70.01	6.42	4.07	−0.37	−0.76	−0.17
39	Deep groundwater	−8.85	−61.73	5.38	9.07	−0.35	−0.30	−0.30
40	Deep groundwater	−8.71	−63.48	7.67	6.2	0.07	0.18	0.90
41	Deep groundwater	−9.47	−67.58	6.52	8.18	−0.45	−0.59	−0.14
42	Deep groundwater	−9.89	−71.12	6.34	8	−0.48	−0.70	−0.58
43	Deep groundwater	−8.78	−63.74	8.38	6.5	−0.44	−0.38	1.40
44	Deep groundwater	−10.51	−79.23	2.5	4.85	2.64	−2.18	−0.32
45	Deep groundwater	−10.37	−78.56	2.5	4.4	2.41	−1.68	−1.11
46	Deep groundwater	−8.78	−70.83	3.46	−0.59	0.57	−0.56	−1.19
47	Deep groundwater	−8.5	−62.01	3.85	5.99	2.27	−0.28	−1.05
48	Deep groundwater	−8.55	−65.27	3.52	3.13	1.41	−0.76	−0.77
49	Deep groundwater	−8.57	−66.52	3.02	2.04	0.34	−0.93	0.01

Table 2: Chemical composition of all water samples in the study area.

Number	Elevation (masl)	TDS (mg/L)	PH	K (mmol/L)	Na (mmol/L)	Mg (mmol/L)	Ca (mmol/L)	HCO3 (mmol/L)	Cl (mmol/L)	F (mmol/L)	SO4 (mmol/L)
1	765	413.3	7.26	0.01	0.18	1.10	1.56	1.02	0.04	0.06	0.21
2	745	372.2	7.82	0.02	0.33	0.79	1.55	1.02	0.10	0.11	0.33
3	651	317.4	7.51	0.02	0.40	0.83	1.12	0.73	0.06	0.06	0.28
4	650	424.4	7.69	0.03	0.51	1.08	1.58	1.03	0.10	0.11	0.66
5	851	372.8	7.48	0.02	0.17	0.70	1.71	1.12	0.08	0.11	0.29
6	765	321.3	8.23	0.01	0.11	0.74	1.43	0.94	0.07	0.11	0.26
7	981	697.3	7.54	0.05	1.38	1.40	2.89	1.89	0.32	0.39	1.91
8	−20	1728.6	7.67	0.39	11.29	4.62	2.84	1.86	6.94	0.72	3.66
9	−50	892.2	8.9	0.82	10.20	0.25	0.62	0.41	0.75	0.28	0.72
10	−20	1233.5	7.52	0.29	7.75	2.88	2.30	1.51	1.92	0.72	3.69
11	−60	611.8	8.36	0.16	2.96	1.17	1.50	0.98	0.82	0.22	1.37
12	−50	484	8.17	0.12	2.42	0.89	1.36	0.89	0.93	0.33	0.89
13	−22	945.3	7.49	0.14	3.68	1.26	3.02	1.98	0.96	0.28	1.39
14	−30	366.1	8.05	0.06	1.63	0.58	1.07	0.70	0.28	0.11	0.31
15	−23	748.4	7.68	0.08	2.23	1.11	2.85	1.87	0.96	0.17	0.66
16	−18	643.9	7.62	0.02	0.09	3.22	1.40	0.92	0.59	0.39	0.59
17	−13	365.8	7.6	0.01	0.09	1.32	1.33	0.87	0.39	0.33	0.63
18	−20	872.8	7.59	0.10	2.91	1.60	3.40	2.23	2.52	0.33	2.23
19	−30	482.4	7.97	0.16	1.63	1.46	0.99	0.65	0.37	0.17	0.49
20	862	504.2	7.87	0.05	0.49	0.90	2.34	1.53	0.48	0.22	0.82
21	230	347.2	5.89	0.02	0.45	0.66	1.47	0.96	0.10	0.11	0.46
22	650	414	7.6	0.05	0.85	0.91	1.54	1.01	0.18	0.17	0.84
23	660	351.2	7.87	0.05	0.28	0.79	1.43	0.93	0.08	0.06	0.54
24	750	452.3	7.31	0.04	0.31	1.53	1.43	0.93	0.11	0.17	0.46
25	720	629.2	7.92	0.16	1.94	1.12	2.31	1.51	0.80	0.17	1.64
26	921	723	7.69	0.06	2.80	1.27	2.51	1.64	0.93	0.22	1.81
27	1	677.4	7.65	0.31	4.94	1.03	1.45	0.95	2.65	0.17	1.73
28	821	692.2	8	0.03	2.81	0.95	2.61	1.71	0.89	0.28	1.67
29	−660	303.7	9.08	0.18	3.93	0.38	0.16	0.11	0.20	0.17	1.51
30	−510	474	7.74	0.09	1.33	0.98	1.62	1.06	0.27	0.44	0.38
31	−500	451.2	5.81	0.03	1.27	0.68	1.81	1.19	0.45	0.22	0.55
32	−600	435.1	7.36	0.02	0.70	1.04	1.61	1.06	0.20	0.33	0.26
33	−650	351.1	7.19	0.18	0.27	0.64	1.48	0.97	0.14	0.17	0.34
34	−402	565.3	7.8	0.25	7.07	0.09	0.07	0.05	0.31	0.39	0.20
35	−436	477.9	8.18	0.28	4.72	0.28	0.41	0.27	0.32	0.22	0.24
36	−470	365.6	7.56	0.03	0.53	0.61	1.68	1.10	0.21	0.17	0.78
37	−470	441.7	7.4	0.02	0.73	1.00	1.67	1.09	0.18	0.28	0.29
38	−420	404.5	7.31	0.02	0.16	1.16	1.55	1.02	0.25	0.33	0.03
39	−320	421.1	7.31	0.01	0.18	1.13	1.72	1.12	0.18	0.28	0.45

Table 2: Continued.

Number	Elevation (masl)	TDS (mg/L)	PH	K (mmol/L)	Na (mmol/L)	Mg (mmol/L)	Ca (mmol/L)	HCO3 (mmol/L)	Cl (mmol/L)	F (mmol/L)	SO4 (mmol/L)
40	−310	838.3	7.15	0.13	2.30	1.27	3.64	2.38	1.96	0.22	2.26
41	−423	425.7	7.67	0.02	0.64	1.10	1.54	1.01	0.21	0.28	0.37
42	−460	378.7	7.46	0.01	0.30	1.03	1.38	0.90	0.14	0.11	0.20
43	−330	632.4	7.42	0.02	0.39	1.83	2.72	1.79	1.51	0.61	1.07
44	−140	989.7	8.56	0.56	12.24	0.02	0.11	0.07	0.42	0.61	0.02
45	−280	891.6	8.8	0.69	10.27	0.09	0.12	0.08	0.23	0.22	0.03
46	−260	469.7	8.35	0.20	4.91	0.17	0.42	0.28	0.27	0.17	0.40
47	−150	892.2	6.87	0.59	8.79	0.71	1.03	0.67	1.72	0.00	1.39
48	−210	787.3	7.23	0.23	6.46	0.58	1.35	0.89	0.77	0.28	0.02
49	−250	660.7	7.41	0.02	0.10	1.95	2.46	1.61	0.35	0.22	0.03

Table 3: Rainfall weighted average of hydrogen and oxygen isotopes in the Jiaozuo area [1].

Meteorological observatory	Elevation (masl)	Sample number	δ^{18}O (‰)	δ^{2}H (‰)
Jiaozuo area	80	13	−6.50	−42.05

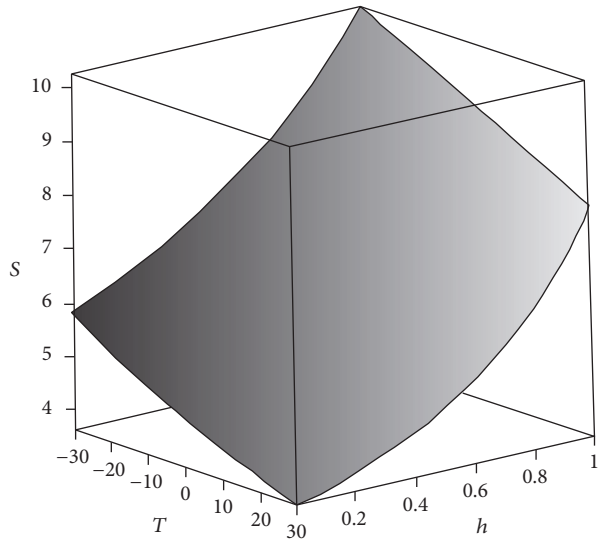

Figure 2: Slope of evaporation line versus temperature and humidity.

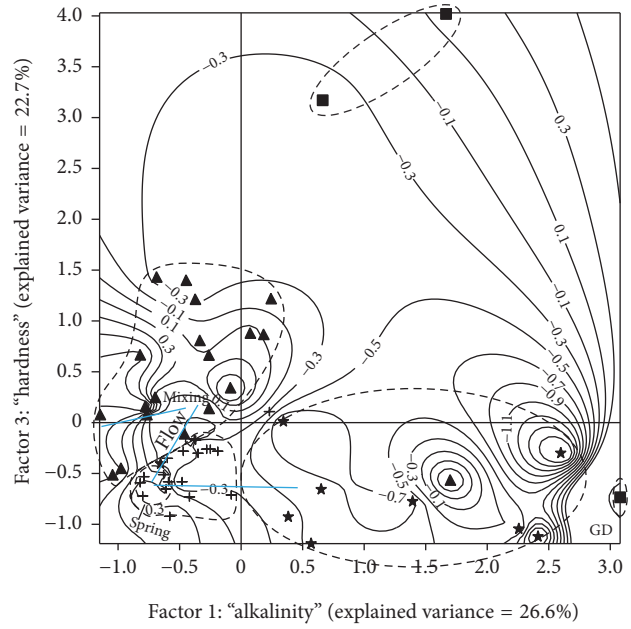

Figure 3: Loadings of the first and third factors.

where f is the fractionation of the remaining water, the fractionation factor coefficient α is the liquid to the vapor state ($\alpha^{*} = 1/\alpha$), T is the air temperature, and h is the air relative humidity.

Formula (2) is simulated in Figure 2. The evaporation line slope gradually decreases with an increase in temperature, whereas the evaporation line slope gradually increases with an increase in humidity. The difference between temperature and humidity is significant in different areas and times. Therefore, the average annual temperature and humidity are used to calculate the evaporation line, which is reasonable. Surface water evaporation line can be calculated according to the S value and the weighted average of rainfall hydrogen and oxygen isotope. The average surface air temperature is 14.3°C, and the average relative air humidity is 0.60 in the Jiaozuo area from 1978 to 1999. Accordingly, the evaporation line slope S can be calculated as 5.84.

The precipitation isotopes in the Jiaozuo area are shown in Table 3. According to the hydrogen and oxygen isotopic weighted average of rainfall in the Jiaozuo Station, the evaporation line is as follows: $\delta D = 5.84\delta^{18}O - 4.09$, which is basically identical with the measured values fitted in the study of Wang [24].

4.2. Factor Analysis. R factor analysis is executed to all parameters [total dissolved solid (TDS), pH, K, Na, Mg, Ca, HCO_3, Cl, F, SO_4, δ^{18}O, δD, and ^{3}H] of the water samples (49 samples). The cumulative contribution rate of the first four factors, which can explain the most original data information, is 84%. The KMO index value is 0.91. The eigenvalues of the first four factors are 4.585, 2.912, 2.318, and 1.110. The HCO_3^{-} and Na^{+} load of the first factor is more than 0.6, which reflects the groundwater alkalinity distribution. This factor is defined as the "alkalinity" factor (Figure 3).

The third factor possesses a high positive load of Ca^{2+} and Mg^{2+}, reflecting the groundwater hardness distribution, which is defined as "hardness" factor. The δ^{2}H and δ^{18}O load of the second factor is more than 0.9, which indicates the information of groundwater-recharging source. The second factor is a fraction distribution in shallow groundwater and surface water, in which the surface water supply is dominant. The second factor exhibits a negative fraction distribution in spring and deep groundwater, which reveals the groundwater-recharging characteristics in the northern mountain area.

5. Discussion

5.1. Karst Water Recharge Source. This study simulates the δD and δ^{18}O distribution characteristics of groundwater in different residual water ratios (f) and air relative humidity conditions according to Formula (2) in the Jiaozuo area. Figure 4 depicts that the slope of the evaporation line becomes gradually close to the atmospheric precipitation line as the humidity increases. When the humidity (h) is

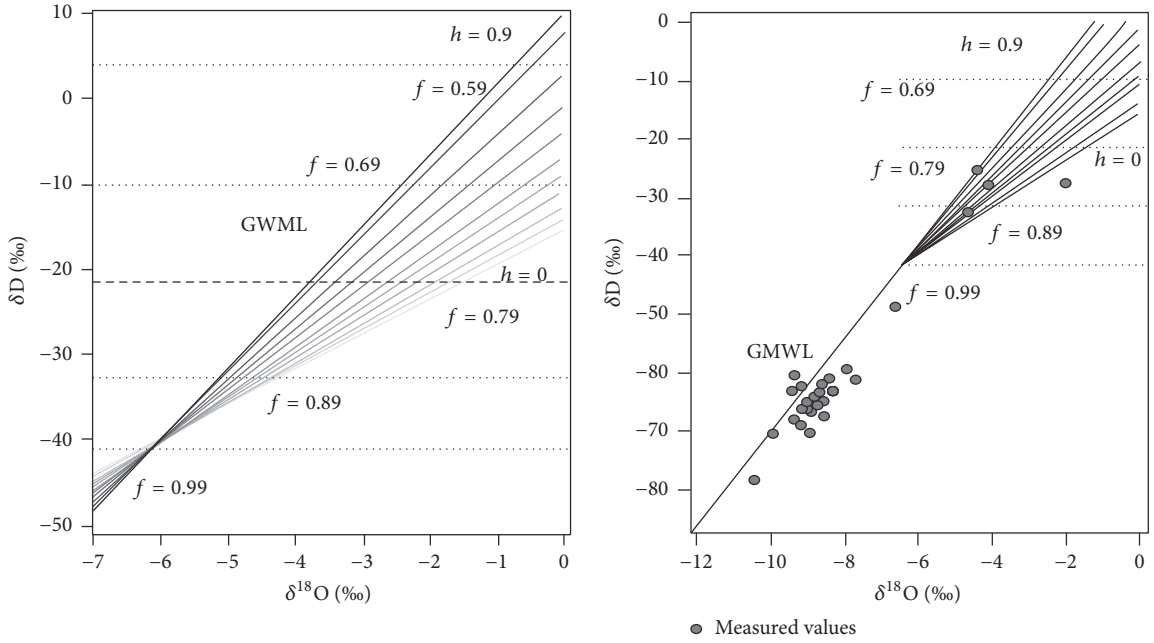

Figure 4: Atmospheric relative humidity versus δD and δ^{18}O values (GMWL is the global meteoric water line).

0.9, the evaporation line almost overlaps the atmospheric precipitation line. Evaporation for different humidity values embodies the same rule that δD and δ^{18}O always change at the right top along the trend line. With an increment in the residual water ratio, the δD and δ^{18}O values of water become gradually close to the supply source. When f is 100%, the water that does not experience evaporation directly accepts the rain supply. Figure 4 also shows that only a minority of the surface water samples become close to the local atmospheric rainfall recharge scope, which mainly falls in the interval of relative humidity from 0 to 0.9 and the remaining water ratio (f) from 79% to 99%. However, most of the groundwater samples clear off the evaporation interval that falls in the lower right interval.

It shows that there are good correlations about HCO_3, Na, Ca, Mg, and δ^{18}O and no correlations between Ca and Na in the deep groundwater, indicating that the Ca^{2+} and Na^+ exchanging interaction plays a key role, leading the balance equation of carbonate dissolving to increasing HCO_3^- direction. From Mount Taihang to coal-mining district, the first factor scores and the third factor scores increase gradually, indicating salt accumulating gradually and groundwater lateral recharging process. Groundwater lies the starting end of runoff evolution, which is often considered as recharging source [25]. The contour map of the second factor scores shows that karst water and spring are at the same area, indicating karst water recharging process (Figure 3).

Figure 5 presents that the evaporation line is approximately a parallel global rain line after the water body is evaporated by 11% or 21%, which indicates that the global rain line can analyze the groundwater recharge source. The calculation result according to the measured values of δ^{18}O of the deep groundwater in the Jiaozuo mining area shows that the δ^{18}O value of the rainfall of the recharging area is obviously lower than the δ^{18}O weighted average (−6.50‰) of rainfall in the Jiaozuo area. The measured tritium values of the deep groundwater samples are greater than 3 TU. This finding indicates that another recharge source of the deep groundwater exists in the Jiaozuo mining area.

A significant linear relationship is determined between δ^{18}O and the elevation of spring outcrop. The topography increases per 100 m, and the δ^{18}O value reduces by 0.23‰ on average. The relationship (Figure 4) implies an obvious oxygen isotope elevation effect.

$$\delta^{18}\text{O (‰)} = -0.0023h - 7.6916, \quad (4)$$

where h is the spring water level. The δ^{18}O value is converted into Formula (4) to calculate the rainfall recharge elevation, which is approximately from 400 to 800 m (Figure 6). This result indicates that the karst water in the mining area is recharged mainly from the altitude of 400 m above the region, where carbonate-exposed areas exist in the Northern Taihang Mountain. The δ^{18}O versus D-excess (D-excess = δD − 8δ^{18}O) also reveals that the deep groundwater in the coal-mining area mainly accepts the recharge of groundwater in the northern mountain area (Figure 7).

5.2. Conceptual Model. In the coal-mining exploring district, the runoff recharging path of groundwater can be described by a conceptual model (Figure 8). The leakage section of the Dan River features the power and geological conditions of infiltration recharge. The Cl ion concentration and the TDS

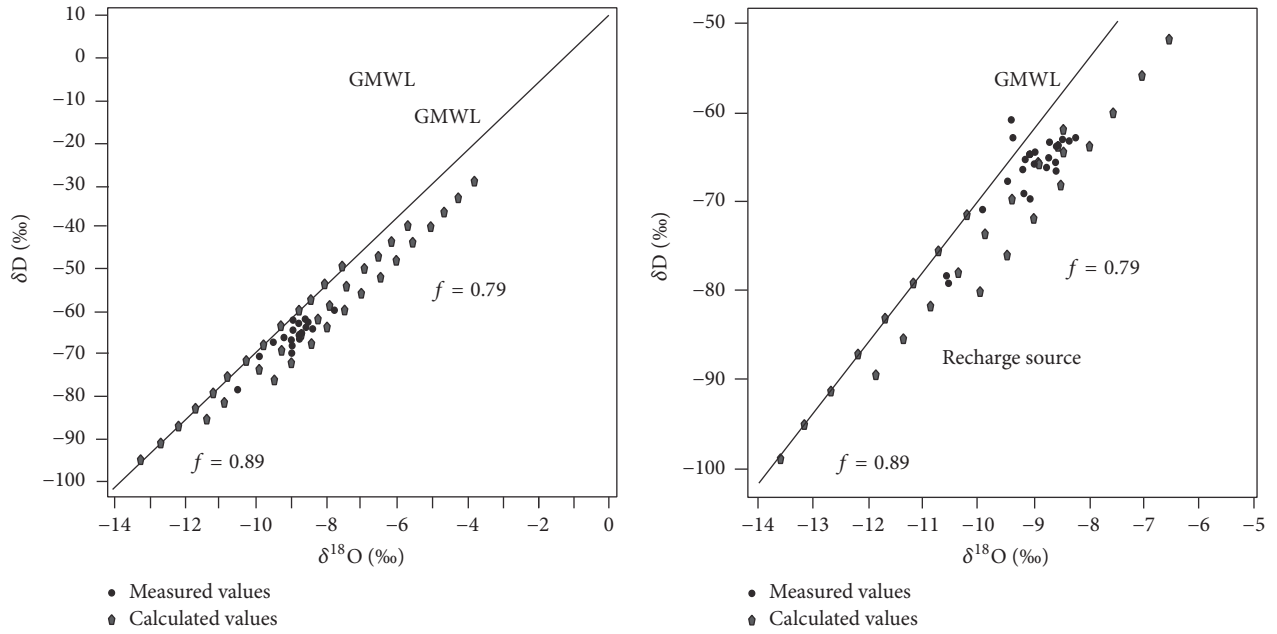

Figure 5: δD and δ^{18}O values of groundwater explaining the process in the Jiaozuo mining district. From the north to the collection of Taihang Mountains.

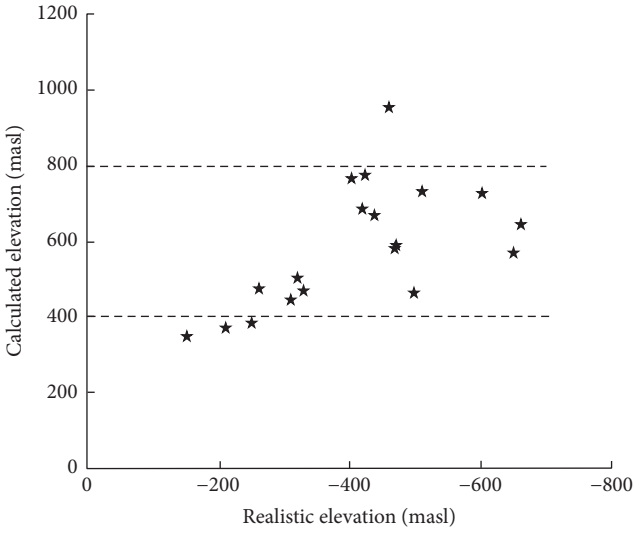

Figure 6: Real elevation versus calculated recharge elevation of deep groundwater.

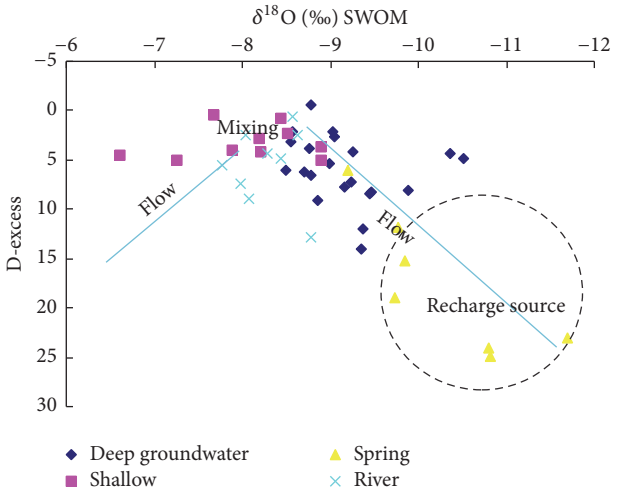

Figure 7: δ^{18}O versus D-excess plot showing the stable isotope composition of water in the study area.

content in the groundwater present a trend gradually from the Dan River to the western mining area, which reflects the water-rock interaction during runoff. The groundwater in the western mining area is mainly affected by the supply of the Dan River. The groundwater in the eastern mining area is mainly recharged from the groundwater of the northern mountain area. The bare limestone stratum in the southern foothills of the Mount Taihang receives the precipitation recharge. One part of the karst water recharges the limestone aquifer in the piedmont plain through a strong leakage zone in the runoff area, while another part supplies the rivers of the mountainous areas in the form of springs.

6. Conclusion

The local evaporation line is established based on hydrogen and oxygen isotope tracer theory and measured rainfall data. This line inversely simulates the groundwater recharge area. The result indicates that the main recharge area of karst water is likely to come from the Shanxi Plateau area. Nevertheless, the groundwater migration mechanism needs further study. The study results can provide new ideas for the prevention

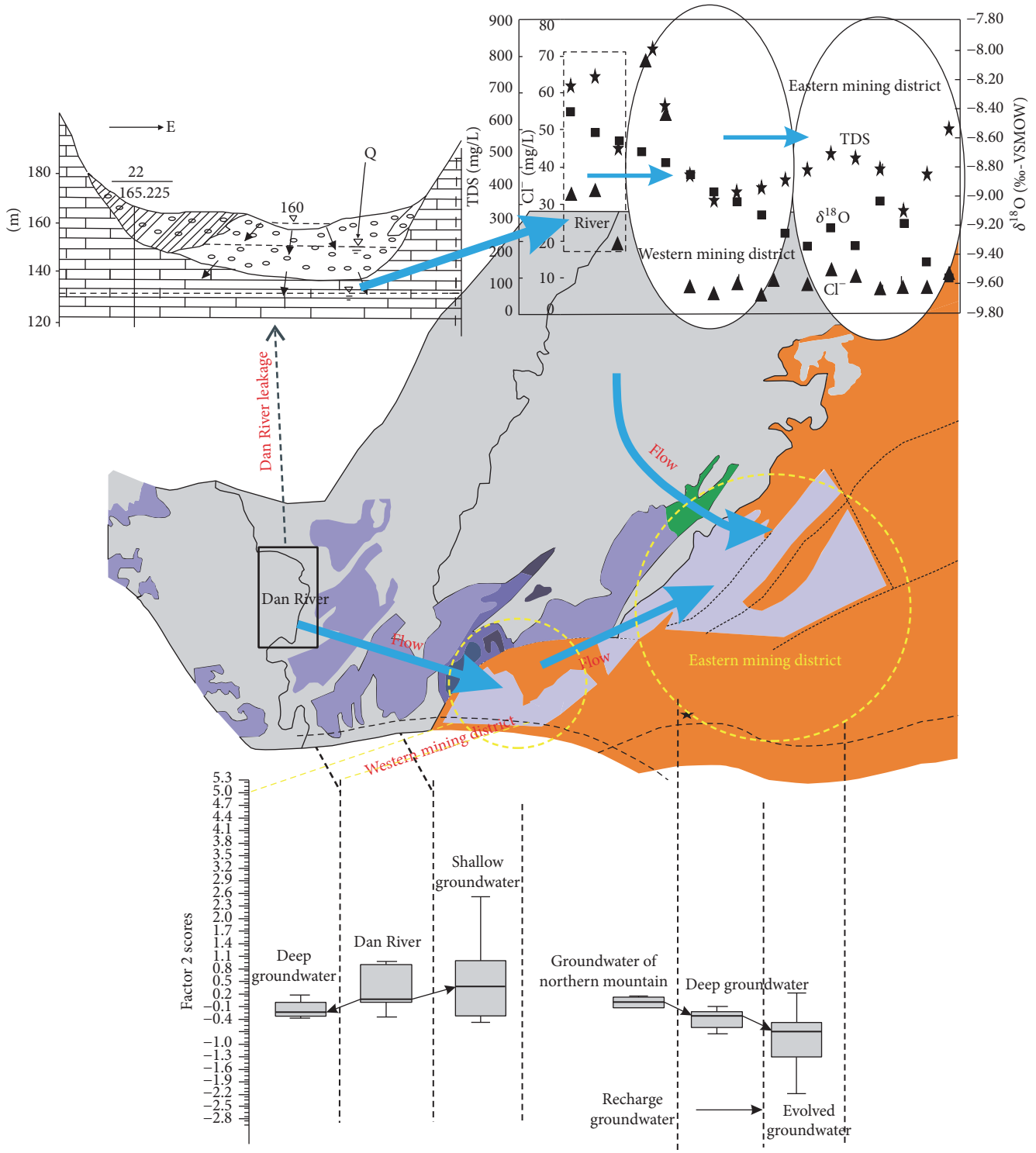

Figure 8: Conceptual model of the groundwater flow path in the study area.

and control of water disasters and management of local water resources.

Conflicts of Interest

The authors declare that they have no conflicts of interest.

Acknowledgments

This work was financially supported by the Science and Technology Key Research Project of the Education Department of Henan, China (nos. 13A170313, 14A510022), China Postdoctoral Science Foundation (no. 182497), and the Technological

Innovation Team of Colleges and Universities in Henan, China (Grant 15IRTSTHN027).

References

[1] J. G. Pei and C. S. Tong, "The study of precipitation hydrogen and oxygen stable isotopic composition in the Jiaozuo area," in *Proceedings of the 2nd National Isotope Hydrology Method Academic Seminars*, vol. 2, pp. 236–240, 1993.

[2] V. Carucci, M. Petitta, and R. Aravena, "Interaction between shallow and deep aquifers in the Tivoli Plain (Central Italy) enhanced by groundwater extraction: a multi-isotope approach and geochemical modeling," *Applied Geochemistry*, vol. 27, no. 1, pp. 266–280, 2012.

[3] J. Ma, D. Li, J. Zhang, W. M. Edmunds, and C. Prudhomme, "Groundwater recharge and climatic change during the last 1000 years from unsaturated zone of SE Badain Jaran Desert," *Chinese Science Bulletin*, vol. 48, no. 14, pp. 1469–1474, 2003.

[4] J. Ma, W. M. Edmunds, J. He, and B. Jia, "A 2000 year geochemical record of palaeoclimate and hydrology derived from dune sand moisture," *Palaeogeography, Palaeoclimatology, Palaeoecology*, vol. 276, no. 1-4, pp. 38–46, 2009.

[5] H. Qian, J. Wu, Y. Zhou, and P. Li, "Stable oxygen and hydrogen isotopes as indicators of lake water recharge and evaporation in the lakes of the Yinchuan Plain," *Hydrological Processes*, vol. 28, no. 10, pp. 3554–3562, 2014.

[6] A. Murad, "Evolution of isotopic compositions in groundwater of the area between the Gulf of Oman and the Arabian Gulf," *Chinese Journal of Geochemistry*, vol. 29, no. 2, pp. 152–156, 2010.

[7] S. Chidambaram, M. V. Prasanna, A. L. Ramanathan et al., "A study on the factors affecting the stable isotopic composition in precipitation of Tamil Nadu, India," *Hydrological Processes*, vol. 23, no. 12, pp. 1792–1800, 2009.

[8] L. Dassi, "Use of chloride mass balance and tritium data for estimation of groundwater recharge and renewal rate in an unconfined aquifer from North Africa: a case study from Tunisia," *Environmental Earth Sciences*, vol. 60, no. 4, pp. 861–871, 2010.

[9] J. J. Gibson, M. A. Sadek, D. J. M. Stone et al., "Evaporative isotope enrichment as a constraint on reach water balance along a dryland river," *Isotopes in Environmental and Health Studies*, vol. 44, no. 1, pp. 83–98, 2008.

[10] Y. Liu, N. Fan, S. An et al., "Characteristics of water isotopes and hydrograph separation during the wet season in the Heishui River, China," *Journal of Hydrology*, vol. 353, no. 3-4, pp. 314–321, 2008.

[11] H. R. Gui, L. W. Chen, and X. M. Song, "Drift characteristics of groundwater hydrogen and oxygen stable isotopes in the wanbei mining area," *Journal of Harbin Technology Institute*, vol. 37, no. 1, pp. 111–114, 2005.

[12] L. W. Chen, H. R. Gui, and X. X. Yan, "The oxygen stable isotopic composition and water cycle tracer of deep groundwater hydrogen," *Journal of coal*, vol. 33, no. 10, pp. 1107–1111, 2008.

[13] H. Dou, Z. Ma, H. Cao, F. Liu, W. Hu, and T. Li, "Application of isotopic and hydro-geochemical methods in identifying sources of mine inrushing water," *Mining Science and Technology*, vol. 21, no. 3, pp. 319–323, 2011.

[14] G. C. Wang and J. S. Li, "Groundwater flow system identification and the preliminary study of the karst development law in the Pingdingshan mining area," *Hydrological Geology and Engineering Geology*, vol. 19, no. 4, pp. 16–18, 1992.

[15] G. X. Yin and Z. S. Li, *Prevention and Pollution of Groundwater*, Chinese Environmental Science and Press, Beijing, China, 2005.

[16] H. F. Kaiser, "The varimax criterion for analytic rotation in factor analysis," *Psychometrika*, vol. 23, no. 3, pp. 187–200, 1958.

[17] H. H. Harman, *Modern Factor Analysis*, University of Chicago Press, Chicago, Ill, USA, 1960.

[18] I. M. Farnham, K. J. Stetzenbach, A. K. Singh, and K. H. Johannesson, "Deciphering groundwater flow systems in Oasis Valley, Nevada, using trace element chemistry, multivariate statistics, and geographical information system," *Mathematical Geology*, vol. 32, no. 8, pp. 943–968, 2000.

[19] I. M. Farnham, K. H. Johannesson, A. K. Singh, V. F. Hodge, and K. J. Stetzenbach, "Factor analytical approaches for evaluating groundwater trace element chemistry data," *Analytica Chimica Acta*, vol. 490, no. 1-2, pp. 123–138, 2003.

[20] K. J. Stetzenbach, V. F. Hodge, C. Guo, I. M. Farnham, and K. H. Johannesson, "Geochemical and statistical evidence of deep carbonate groundwater within overlying volcanic rock aquifers/aquitards of southern Nevada, USA," *Journal of Hydrology*, vol. 243, no. 3-4, pp. 254–271, 2001.

[21] R. K. Steinhorst and R. E. Williams, "Discrimination of groundwater sources using cluster analysis, MANOVA, Canonical Analysis and Discriminant Analysis," *Water Resources Research*, vol. 21, no. 8, pp. 1149–1156, 1985.

[22] M. A. Majoube, "Fractionnement en oxygene-18 et endeuterium entre leau et sa vapeur," *Journal of Chemical Physics*, vol. 68, pp. 1423–1436, 1971.

[23] P. Huang and J. Chen, "Recharge sources and hydrogeochemical evolution of groundwater in the coal-mining district of Jiaozuo, China," *Hydrogeology Journal*, vol. 20, no. 4, pp. 739–754, 2012.

[24] F. G. Wang, *Isotopic technique was applied for the water cycle characteristics research in the lower reaches section of the Yellow River (henan section) [Ph.D. thesis]*, 2006.

[25] J. W. Lloyd and J. A. Heathcoat, *Natural Inorganic Chemistry in Relation to Ground Water*, Clarendon Press, Oxford, UK, 1985.